

Occlusion-Aware SORT: Observing Occlusion for Robust Multi-Object Tracking

Chunjiang Li¹ Jianbo Ma² Li Shen¹ Yanru Chen^{1*} Liangyin Chen¹

¹College of Computer Science, Sichuan University, Chengdu, China

²Institute of Optics and Electronics, CAS, Chengdu, China

lichunjiang@stu.scu.edu.cn, {chenyanru, chenliangyin}@scu.edu.cn

Abstract

Multi-object tracking (MOT) involves analyzing object trajectories and counting the number of objects in video sequences. However, 2D MOT faces challenges due to positional cost confusion arising from partial occlusion. To address this issue, we present the novel Occlusion-Aware SORT (OA-SORT) framework, a plug-and-play and training-free framework that includes the Occlusion-Aware Module (OAM), the Occlusion-Aware Offset (OAO), and the Bias-Aware Momentum (BAM). Specifically, OAM analyzes the occlusion status of objects, where a Gaussian Map (GM) is introduced to reduce background influence. In contrast, OAO and BAM leverage the OAM-described occlusion status to mitigate cost confusion and suppress estimation instability. Comprehensive evaluations on the DanceTrack, SportsMOT, and MOT17 datasets demonstrate the importance of occlusion handling in MOT. On the DanceTrack test set, OA-SORT achieves 63.1% and 64.2% in HOTA and IDF1, respectively. Furthermore, integrating the Occlusion-Aware framework into the four additional trackers improves HOTA and IDF1 by an average of 2.08% and 3.05%, demonstrating the reusability of the occlusion awareness.

1. Introduction

Multi-Object Tracking (MOT) is used to capture the trajectories of objects in video footage or webcam streams. The fundamental objective is to assign a unique identifier to each detected object [34]. The field has a variety of applications, including the analysis of object movements [22], the tracking of changes in human postures [14], and the accurate counting of objects [68]. Despite significant progress in this area, MOT still faces challenges brought by occlusion.

Currently, position association (widely used in MOT) remains a pivotal element for tracking objects across successive frames. The majority of trackers [2, 4, 52, 62] rely on

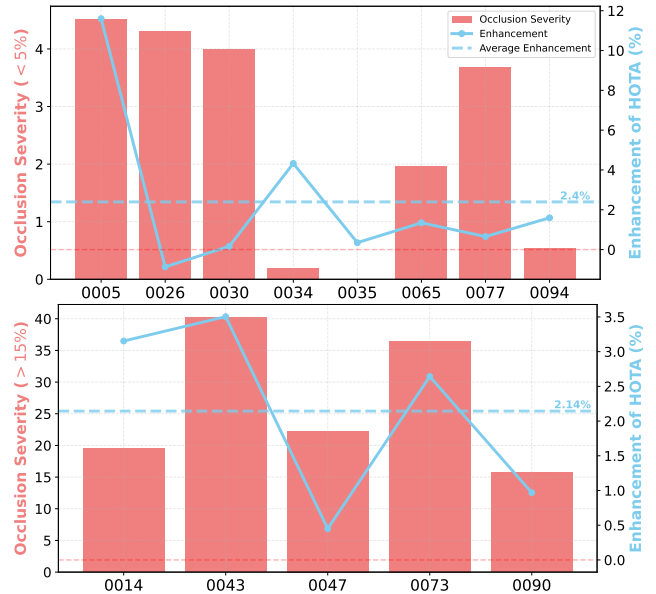


Figure 1. Performance improvement of OA-SORT over baseline (Hybrid-SORT) on the DanceTrack validation set under different occlusion severity, where the horizontal axis represents the video sequence number. The severity is defined as the proportion of object instances whose average occlusion ratio (Eq. 4) exceeds 0.75.

position association, which utilizes motion cues such as velocity and acceleration to predict the objects' positions in a video sequence. The position association consists of three main components: position predictor [11, 24], spatial consistency metrics [58, 60], and the Hungarian algorithm [28]. However, the tracking process often presents challenges due to partial occlusion. In terms of detection, it becomes difficult to differentiate between the foreground (*i.e.*, the object itself) and the background when objects of the same category exhibit occlusion behavior. This ultimately leads to inaccurate detection. Moreover, discrete and linear position predictors (such as Kalman Filter [24], KF) are severely affected by frequent inaccurate detections. The impact is more pronounced when the motion of an object is irregular and variable, such as during non-linear posture changes. In

*Corresponding author

the subsequent process of data association between detection and trajectory estimation, unstable predictions and inaccurate detections can easily lead to serious cost confusion. Cost confusion refers to the ambiguity in the generated position cost matrix, which cannot accurately and stably reflect the affinity between detection and estimation. This often leads to frequent or even permanent identity exchanges.

To alleviate this impact, many methods have introduced additional cues, such as appearance features [1, 51, 54, 61], motion direction [6, 37], and detection confidence [25, 62]. These additional cues improve association performance to some extent. However, inaccurate detections caused by occlusion often compromise the reliability of additional cues. In terms of appearance features, the features' reliability decreases due to inaccurate detections, leading to feature cost confusion. The feature of an occluded object is easily influenced or even replaced by the objects in front of it. Secondly, while motion direction can effectively reduce failed matches during occlusion, cost confusion persists. Similarly, confidence is sensitive to occlusion, and when an object occludes another, the score of the occluded object is affected. In conclusion, while these additional cues enhance association accuracy to a certain extent, cost confusion due to occlusion remains a prevalent issue.

To this end, the paper focuses on mitigating positional cost confusion arising from occlusion and introduce a novel approach to observing the occlusion status of objects and employing this to form an occlusion-aware tracking framework. Firstly, the *Occlusion-Aware Module (OAM)* is designed to observe and estimate the occlusion status of objects, *i.e.*, obtaining the occlusion coefficient that reflects occlusion severity. During the calculation process, the *Gauss map (GM)* is introduced to refine the coefficient. On this basis, two new components are proposed, *i.e.*, *Occlusion-Aware Offset (OAO)* and *Bias-Aware Momentum (BAM)*. Finally, a novel occlusion-aware tracking framework, *Occlusion-Aware SORT (OA-SORT)*, is formed by combining these components as shown in Fig. 2. Specifically, OAO integrates the occlusion coefficient into the spatial consistency metric to mitigate cost confusion, where the coefficient is used to describe the estimations from the position predictor. BAM aims to reduce the impact caused by inaccurate detections by combining the occlusion coefficient with the spatial consistency metric, thereby enhancing robustness of the position predictor. The occlusion coefficient is used to describe the latest observation of trajectories. Finally, on the DanceTrack, OA-SORT achieves 63.1%, 48.5%, and 64.2% in HOTA, AssA, and IDF1. Our contributions are summarized as follows:

- The presented OAM observes and evaluates the occlusion status, and GM is introduced to reduce background interference.
- Based on the OAM, the designed OAO and BAM miti-

gate cost confusion and optimize the predictor's estimations, demonstrating that integrating occlusion status effectively reduces occlusion-induced issues. Building on those, we design the occlusion-aware framework, OA-SORT, achieving outstanding performance across various occlusion scenarios, as shown in Fig. 1.

- OAM, OAO, BAM, and occlusion-aware framework can be easily integrated into diverse association strategies and architectures. Experiments on DanceTrack show that occlusion-aware framework brings benefits for the four association methods [6, 31, 52, 62] with improvements of average +2.08% HOTA and +3.05% IDF1. Further ablation studies, including other trackers [2, 6, 45, 62], on the DanceTrack validation set verify the generalization and effectiveness of OAO and BAM. The rationality of the occlusion-aware framework is fully explained.

2. Related work

Association [2, 3, 36, 40, 62] aims to match identical objects across frames. For association based on position information, two primary paradigms are commonly employed.

Position-Association relies exclusively on positional information to associate trajectories with detected objects. To address the non-linearity limitations of KF, some works propose improved prediction methods, such as the Unscented KF [23], Extended KF [27], and NSA KF [11]. Although these extensions improve motion modeling accuracy, they still rely on KF's motion estimates. Alternatively, some methods [40, 65] integrate learnable models to capture non-linear motion factors. However, occlusion remains an unresolved problem in the field. To address this challenge, some methods [19, 46, 69] have been designed to incorporate more comprehensive strategies or components. For example, Stadler *et al.* [46] employed the objects' active or inactive states to determine the occlusion relationships, subsequently analyzing the velocity of inactive objects to predict their probable positions in the current frame. This approach indirectly models occlusion rather than explicitly estimating it. Conversely, Hibo *et al.* [69] proposed a compensation tracker that recovers lost objects using motion compensation. More recently, methods [6, 31, 52, 58] attempt to address occlusion in MOT by analyzing the object motion or exploiting depth information. However, these methods still suffer from the cost confusion caused by occlusion, and this problem is more pronounced when objects exhibit similar motions. In this paper, we directly analyze the occlusion severity to mitigate occlusion-induced cost confusion.

Position-and-Feature-Association combines appearance features [7, 21, 50, 64, 67] with positional estimations to construct new trackers [1, 12, 51, 54, 61, 66], thereby effectively extending the maximum allowable loss time for objects. For instance, Wang *et al.* [54] combined FPN [30] with a multiscale anchor-based detector to detect objects

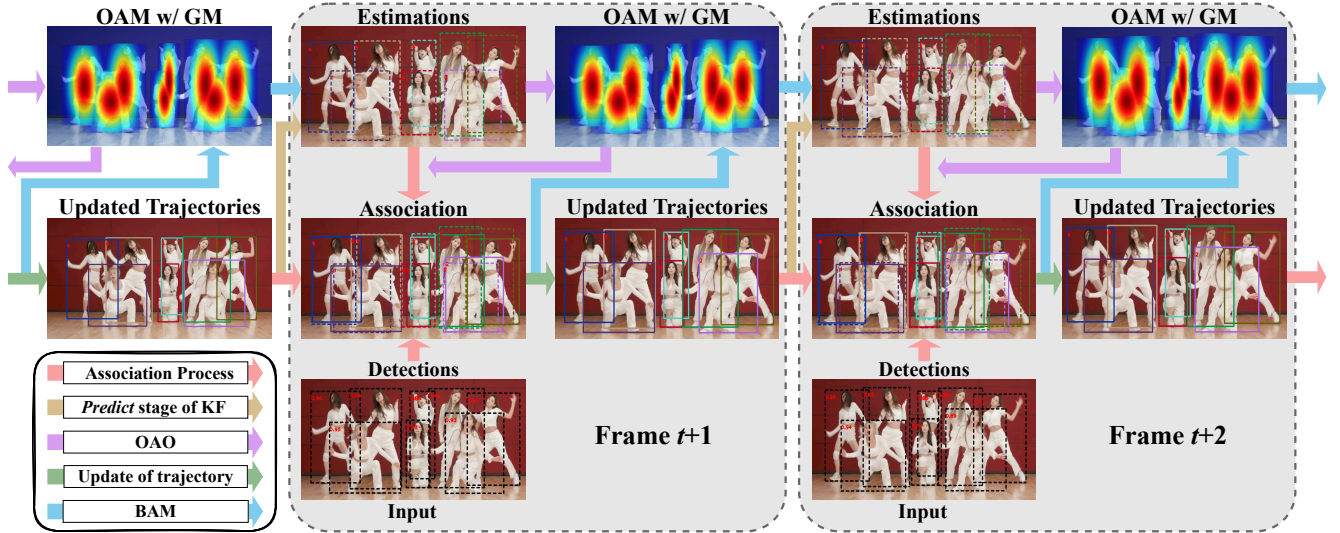


Figure 2. Pipeline of OA-SORT (Sec. 4.4). Before association, OAO (Sec. 4.2) leverages the occlusion coefficient, which is derived from KF’s estimation by OAM (Sec. 4.1) with GM (Sec. 4.1.3), to refine the positional cost between trajectories and high-confidence detections. During the update stage, BAM (Sec. 4.3) integrates the occlusion coefficient from the latest observation with IoU to refine the KF update.

and extract features. To enhance performance, global and local appearance features [49] are extracted using AlphaPose [13], which estimates key points (*e.g.*, hands) of objects (*e.g.*, pedestrians) and matches detections with trajectories. Although this approach enhances association robustness, the Position-and-Feature-Association paradigm faces similar challenges regarding positional consistency as the Position-Association paradigm. Consequently, we focus on handling occlusion in the context of Position-Association.

3. Thinking for Occlusion

3.1. Preliminaries

KF is a linear estimator for dynamical systems. It utilizes the state estimates from the previous time step and the current measurement to predict the object’s next state. In tracking, two tasks need to be accomplished: *predict* and *update*. The *update* stage at time t uses the actual observation \mathbf{z}_t of a trajectory to obtain the posterior state estimate $\hat{\mathbf{x}}_{t|t}$ at time t , where the observation corresponds to a detection associated with the trajectory. Mathematically,

$$\hat{\mathbf{x}}_{t|t} = \hat{\mathbf{x}}_{t|t-1} + \mathbf{K}_t (\mathbf{z}_t - \mathbf{H}_t \hat{\mathbf{x}}_{t|t-1}), \quad (1)$$

where \mathbf{H} denotes the observation model, and \mathbf{K} is the Kalman Gain matrix. \mathbf{K} is a key process parameters that integrates noise, ensuring the smoothness and stability of estimates.

IoU is a critical metric in MOT for assessing the spatial relationship between estimated and detected bounding boxes, describing the position affinity. In this paper, $C_{IoU}(\cdot, \cdot) \in [0, 1]$ is used to present the computed IoU value.

3.2. Influence of Occlusion for Position Association

To begin with, we assume that the practical detected and estimated positions of an object follow $d = P + \Delta_d$ and $e = P + \Delta_e$, where P denotes the actual position of the object; Δ_d and Δ_e indicate the detection and estimation errors. Under partial occlusion, the loss of appearance features increases the detection error, *i.e.*, $\Delta_d \uparrow = \Delta_d + \Delta_{d,occ}$. In a sufficiently short time, the $C_{IoU}(d, e)$ might change suddenly because of inaccurate detection. Over a long time, due to inaccurate detections occurring frequently, $\Delta_e \uparrow = \Delta_e + \Delta_{e,occ}$ accumulates to become unstable, ultimately resulting in a degradation or fluctuations in $C_{IoU}(d, e)$. Those phenomena easily cause cost confusion.

Herein, we assume that object i and j of similar size are spatially close in a moment and object i is occluded by object j , *i.e.*, $C_{IoU}(P_i, P_j)$ may approach 1. Due to the instability and accumulation of errors, it might become difficult for the IoU metric to evaluate the spatial consistency between detection and estimation. Moreover, the Hungarian algorithm implements the lowest-position-cost mechanism for detection-estimation allocation, where position cost is indicated as $Cost_{IoU}(\cdot, \cdot) = 1 - C_{IoU}(\cdot, \cdot)$. However, due to cumulative errors from inaccurate KF’s estimations, e_i and e_j , and d_i may change such that $Cost_{IoU}(d_j, e_i) < Cost_{IoU}(d_j, e_j)$ or $Cost_{IoU}(d_j, e_i) < Cost_{IoU}(d_i, e_i)$, potentially causing false association. This leads to the exchange of identities between trajectories. Our work focuses on observing occlusion to introduce a new cost for objects and optimize KF’s parameters. Those approach increases $Cost_{IoU}(d_j, e_i)$ and decreasing $Cost_{IoU}(d_i, e_i)$, thereby alleviating cost confusion.

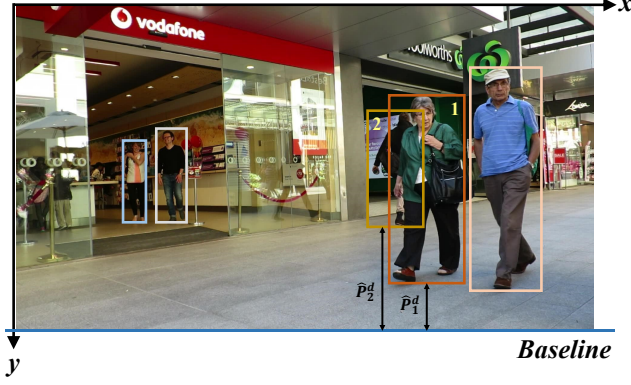


Figure 3. Illustration of the depth relationship. Since the bottom edge of the bounding box is parallel to the *Baseline*, the vertical distance to the *Baseline* is defined as \hat{P}^d .

4. Methodology

In this section, we introduce *occlusion-aware SORT framework (OA-SORT)* as illustrated in Fig. 2. To address the cost confusion, we integrate the *Occlusion-Aware Module (OAM)* into the position association and the Kalman Filter (KF) updating process. *Occlusion-Aware Offset (OAO)* and *Bias-Aware Momentum (BAM)* assist the association and KF updating, respectively.

4.1. Occlusion-Aware Module

4.1.1. Depth Ordering

Most two-dimensional cameras implement surveillance in an overhead (non-vertical) view in real-world scenarios. When a camera captures ground-moving objects (*i.e.*, non-flying) on a plane, the relative depth relationship between objects can be estimated from their bounding box bottom edges [31, 41, 52]. As illustrated in Fig. 3, the position of a bounding box’s bottom edge provides information about its relative depth with respect to the camera. If $\hat{P}_1^d < \hat{P}_2^d$, object #1 is closer to the camera and therefore in front of object #2. Therefore, for any two detected objects i and j ,

$$\left(\hat{P}_i^d < \hat{P}_j^d\right) \Leftrightarrow (\text{Object } i \prec \text{Object } j). \quad (2)$$

This method assist in tracking objects in realistic scenarios and is referred to as *Depth Ordering*. By applying this method, detections can be analyzed to determine the front-and-back relationships between objects. Notably, to avoid fluctuations in the bounding box in actual scenes, a threshold (5) has been set for Depth Ordering to reduce sensitivity, *i.e.*, $\hat{P}_i^d + 5 < \hat{P}_j^d \rightarrow \text{Object } i \prec \text{Object } j$.

4.1.2. Occlusion Coefficient

Based on the Depth Ordering, the overlap between detections is calculated to quantify the occlusion severity, expressed as the Occlusion Coefficient (Oc). Specifically, let

\mathcal{D}_i and \mathcal{D}_j represent the two detections for objects i and j , and $\hat{P}_i^d > \hat{P}_j^d$. The corresponding overlap region is $\mathcal{D}_i \cap \mathcal{D}_j$. Because $\hat{P}_i^d > \hat{P}_j^d$, object i is located behind object j , as defined in Depth Ordering. The $Oc \in [0, 1]$ for object i by object j can be expressed as

$$Oc_i^j = \frac{\mathbf{A}(\mathcal{D}_i \cap \mathcal{D}_j)}{\mathbf{A}(\mathcal{D}_i)}, \quad (3)$$

where $\mathbf{A}(\cdot)$ calculates the pixel count of the region, and the overlap region $\mathcal{D}_i \cap \mathcal{D}_j$ also represents the occlusion region. In practice, an object may be occluded by multiple others. Thus, let $\mathcal{O}_i = \bigcup_{k \in Occ(i)} (\mathcal{D}_i \cap \mathcal{D}_k)$ represent the occluded regions for object i , where $Occ(i)$ denotes the index set of objects that occlude object i . The global occlusion coefficient Oc_i is interpreted as

$$Oc_i = \frac{\mathbf{A}(\mathcal{O}_i)}{\mathbf{A}(\mathcal{D}_i)}. \quad (4)$$

The method computes the occlusion coefficient, which serves for bounding boxes generated by the detector or KF.

4.1.3. Occlusion Coefficient Refinement

The occlusion coefficient Oc may overestimate an object’s occlusion severity, since its bounding box can include background pixels, particularly near the boundaries. To mitigate background influence, we introduce the Gaussian Map (GM) to refine Oc by adaptively weighting each pixel according to its distance from the bounding box center. For an image frame with N detected objects, the GM value $GM_{x,y} \in [0, 1]$ is defined at pixel (x, y) as

$$GM_{x,y} = \max_{n=1}^N \left(e^{-\left(\frac{(x-cx_n)^2}{2(\sigma_n^x)^2} + \frac{(y-cy_n)^2}{2(\sigma_n^y)^2} \right)} \right), \quad (5)$$

where pixel (x, y) is within the detected bounding boxes, (cx_n, cy_n) denotes the centroid of the bounding box of the object n , and (σ_n^x, σ_n^y) are the standard deviations about the detected object category in the horizontal and vertical directions. In this work, σ^x and σ^y are set proportionally to the bounding box width (w) and height (h), ensuring smooth decay of the Gaussian kernel from the center to the edges. The refined occlusion coefficient $\hat{O}c$ for each object i is calculated by

$$\hat{O}c_i = Oc_i \cdot \frac{\sum_{(x,y) \in \mathcal{O}_i} GM_{x,y}}{\mathbf{A}(\mathcal{O}_i)} \quad (6)$$

$$= \frac{\sum_{(x,y) \in \mathcal{O}_i} GM_{x,y}}{\mathbf{A}(\mathcal{D}_i)}, \quad (7)$$

where pixels closer to the object center dominate the occlusion severity, effectively suppressing the influence of the background. Notably, $\hat{O}c_i = 0$ when no occlusion occurs. The complete process of obtaining $\hat{O}c$ constitutes the *Occlusion-Aware Module (OAM)*, corresponding to *OAM w/ GM* in Fig. 2.

4.2. Occlusion-Aware Offset

As discussed above, objects with similar bounding boxes—particularly those in close proximity—exhibit high IoU-based spatial consistency, which can cause position cost confusion. Even when objects are correctly associated with trajectories, their identities may switch due to uncertainty in positional errors. To alleviate this problem, we propose *Occlusion-Aware Offset (OAO)* to integrate the occlusion coefficient into the position cost. Because occlusion often yields inaccurate detections, directly applying OAM to detections is unreliable. This instability arises because the bottom edges of inaccurate detections fluctuate, undermining depth consistency. In contrast, KF not only predicts the position of the trajectory at the next time step using historical motion information but also suppresses the effect of weak noise. Therefore, in this work, OAM is deployed for KF’s estimate \mathbf{X} to generate the occlusion coefficient $\hat{O}c^{\mathbf{X}}$, where \mathbf{X} can be represented using $P + \Delta_e$. By combining C_{IoU} and $\hat{O}c^{\mathbf{X}}$, the final spatial consistency score S is defined as

$$S = \tau \cdot (1 - \hat{O}c^{\mathbf{X}}) + (1 - \tau) \cdot C_{IoU}(\mathcal{D}, \mathbf{X}), \quad (8)$$

where $\tau \in [0, 1]$ represents a coefficient that balances $C_{IoU}(\mathbf{X}, \mathcal{D})$ and $\hat{O}c^{\mathbf{X}}$. Thus, $Cost_{IoU} = 1 - S$ is used to prevent cases where $Cost_{IoU}(d_j, e_i) < Cost_{IoU}(d_j, e_j)$. This process, termed *Occlusion-Aware Offset*, operates on KF’s predictions and is only triggered during the First-stage association for high-score detections.

4.3. Bias-Aware Momentum

Although KF estimates are typically more stable than raw detections, frequent inaccurate detections under occlusion can accumulate errors in the KF, leading to estimation fluctuations. In short time intervals, the KF’s estimate is usually more reliable than newly received low-quality detections. Thus, we design *Bias-Aware Momentum (BAM)* for likely inaccurate detections, *i.e.*, those with low scores. BAM incorporates the occlusion coefficient to evaluate the weighting between the estimation and low-score detection, aiming to suppress abnormal variations in the KF’s motion parameters. Additionally, to comprehensively account for the spatial relevance, the IoU metric [58, 60] is incorporated into the BAM calculation to describe the positional relationship between the estimation and the detection.

It is important to note that BAM is designed to optimize the object’s motion estimation. Thus, at time step t , OAM is used for a trajectory’s latest observation \mathbf{Z}_{t-1} to generate the occlusion coefficient $\hat{O}c^{\mathbf{Z}_{t-1}}$, while the associated low-score detection is the current observation \mathbf{Z}_t . BAM is then calculated as

$$BAM = C_{IoU}(\mathbf{X}_{t|t-1}, \mathbf{Z}_t) \cdot (1 - \hat{O}c^{\mathbf{Z}_{t-1}}). \quad (9)$$

Subsequently, during the *update* stage of KF, \mathbf{Z}_t is optimized to $\hat{\mathbf{Z}}_t$ using BAM as follows:

$$\hat{\mathbf{Z}}_t = BAM \cdot \mathbf{Z}_t + (1 - BAM) \cdot \mathbf{H}_t \mathbf{X}_{t|t-1}. \quad (10)$$

Finally, the posterior state estimate $\mathbf{X}_{t|t}$ at the *update* stage is calculated through

$$\mathbf{X}_{t|t} = \mathbf{X}_{t|t-1} + \mathbf{K}_t (\hat{\mathbf{Z}}_t - \mathbf{H}_t \mathbf{X}_{t|t-1}). \quad (11)$$

Integrating the IoU metrics [58, 60] ensures that, under the occlusion, the greater the difference between the estimation and detection, the smaller the value of BAM. In other words, as the discrepancy between estimate and detection grows, $\hat{\mathbf{Z}}_t$ increasingly depends on the estimation $\mathbf{X}_{t|t-1}$. In conclusion, the KF’s motion parameters can be dynamically adjusted during the *update* stage to suppress fluctuations.

4.4. Association approach

OA-SORT adopts Hybrid-SORT as its baseline, *i.e.*, the association includes three stages: (1) the First-stage association links high-score detections with trajectories, (2) the Second-stage handles low-score detections, and (3) the Third-stage reconnects lost trajectories using their latest observation. Overall, our tracking process is shown in Fig. 2. The integration of OAM, OAO, and BAM follows four main steps: 1) After KF estimates for trajectories, OAM utilizes the estimations to calculate the occlusion coefficients; 2) During the process of association, OAO integrates the calculated occlusion coefficients into the spatial consistency metric; 3) For trajectories associated with low-score detection, BAM uses the occlusion coefficients of trajectories’ latest observations to optimize the KF’s motion parameters; 4) Before the end of the current frame, OAM utilizes the trajectories’ latest observation to calculate the occlusion coefficient for subsequent BAM. In practice, the tracking framework can be integrated into other trackers [2, 6, 31, 45, 52, 62]. Notably, both OAO and BAM modules can operate independently.

5. Experiment

5.1. Experimental Setup

Datasets. We evaluate OA-SORT on three widely used benchmarks: DanceTrack [48], SportsMOT [9], and MOT17 [39]. DanceTrack is a challenging benchmark for MOT in stage performance scenarios. It includes diverse nonlinear motions and frequent partial occlusions, whereas SportsMOT features variable-speed motion and dynamic camera movement. MOT17 comprises pedestrian street scenes with frequent and prolonged occlusions.

Metrics. The metrics in the experiments are defined in CLEAR [26], HOTA [32], and PMDS [43]. Here, \uparrow and \downarrow respectively denote that higher or lower values correspond

to better performance: **HOTA (%)** \uparrow is a higher-order tracking accuracy metric, which represents the performance of detection, association, and localization; **MOTA (%)** \uparrow is a comprehensive evaluation indicator for MOT in combination with missed detection, false detections, and ID switch; **IDF1 (%)** \uparrow measures the accuracy of assigning identities; **AssA (%)** \uparrow measures association accuracy, which is simply the average alignment between matched trajectories.

Implementation Details. The hyperparameters of OA-SORT are the same as those in Hybrid-SORT [58]. In OAM, σ^x is $w/3\sqrt{2}$ and σ^y is $h/3$ for DanceTrack; σ^x is $w/4$ and σ^y is $h/3$ for SportsMOT; σ^x is $w/2$ and σ^y is $h/2$ for MOT17. In OAO, τ is 0.15 for DanceTrack, 0.2 for SportsMOT, and 0.1 for MOT17. τ is empirically tuned between 0.1 and 0.2 to balance precision and robustness across motion patterns. Herein, τ for SportsMOT and MOT17 is empirically set based on average IoU between adjacent frames [9]. All experiments are conducted on a single NVIDIA V100 GPU paired with an Intel Xeon (R) 6130 CPU (2.10 GHz).

5.2. Benchmark Results

DanceTrack. As shown in Tab. 1, OA-SORT achieves consistent gains over the baseline Hybrid-SORT [58] (+0.9 HOTA, +1.1 AssA, +0.1 MOTA, +1.2 IDF1). Improvements in AssA and IDF1 indicate that the occlusion-aware framework effectively mitigates cost confusion and refines KF estimation. Notably, Hybrid-SORT already exploits motion direction cues to mitigate occlusion effects. Additionally, integrating occlusion-awareness into other trackers—ByteTrack (OA-Byte), OC-SORT (OA-OC), SparseTrack (OA-Sparse), and PD-SORT (OA-PD)—consistently improves their performance. Although PD-SORT [52] and SparseTrack [31] leverage pseudo-depth to design spatial consistency index metric (DVIoU) and association strategy (DCM), occlusion-aware framework integration further improves performance. Overall, the results demonstrate that modeling and leveraging occlusion states effectively handle nonlinear and interactive motion scenarios.

SportsMOT. Tab. 2 presents results on SportsMOT. The results show that the occlusion-aware framework remains effective under variable-speed motion and camera-view changes. This effectiveness arises because occlusion evaluation is based on relative positions between objects. Even after short-term camera view changes, relative position can be maintained. Notably, OA-SORT achieves these results without any camera-motion compensation. Additionally, as noted in [9], SportsMOT imposes stricter requirements on IoU and Kalman filter accuracy than DanceTrack. The results further confirm the effectiveness and generalizability of the proposed framework. It effectively enhances tracking robustness under occlusion scenarios involving variable-speed motion and high-intensity camera movement.

Method	HOTA	AssA	MOTA	IDF1
CenterTrack [65]	41.8	22.6	86.8	35.7
FairMOT [61]	39.7	23.8	82.2	40.8
QDTrack [15]	45.7	29.2	83.0	44.8
DST-Tracker [5]	51.9	34.6	84.9	51.0
FineTrack [42]	52.7	38.5	89.9	59.8
DiffusionTrack [33]	52.4	33.5	89.3	47.5
MOTIP [17]	67.5	57.6	90.3	72.2
<i>Same Detection:</i>				
SORT [2]	47.9	31.2	<u>91.8</u>	50.8
StrongSORT++ [12]	55.6	38.6	91.1	55.2
C-BIoU [57]	60.6	45.4	91.6	61.6
MotionTrack2024 [56]	58.2	41.7	91.3	58.6
ETTrack [20]	56.4	39.1	92.2	57.5
C-TWiX [38]	62.1	47.2	91.4	<u>63.6</u>
<i>Integration:</i>				
ByteTrack [62]	47.1	31.5	88.2	51.9
OA-Byte (Ours)	49.0	33.7	89.6	55.9
OC-SORT [6]	54.6	40.2	89.6	54.6
OA-OC (Ours)	56.5	39.6	91.2	57.6
SparseTrack [31]	55.5	39.1	91.3	58.3
OA-Sparse (Ours)	57.8	41.8	91.5	60.2
PD-SORT [52]	58.2	42.1	89.6	57.5
OA-PD (Ours)	60.4	44.9	91.4	60.8
Hybrid-SORT [58]	<u>62.2</u>	<u>47.4</u>	91.6	63.0
OA-SORT (Ours)	63.1	48.5	91.7	64.2

Table 1. Results on DanceTrack test set. The same detection is provided by OC-SORT.

Method	HOTA \uparrow	AssA \uparrow	MOTA \uparrow	IDF1 \uparrow
FairMOT [61]	49.3	34.7	86.4	53.5
QDTrack [15]	60.4	47.2	90.1	62.3
TransTrack [47]	68.9	57.5	92.6	71.5
MeMOTR [16]	70.0	59.1	91.5	71.4
MOTIP [17]	71.9	62.0	92.9	75.0
<i>Same Detection:</i>				
ByteTrack [62]	62.8	51.2	94.1	69.8
OC-SORT [6]	71.9	59.8	94.5	72.2
DiffMOT [35]	72.1	60.5	94.5	72.8
MambaTrack [55]	72.6	60.3	95.3	72.8
Hybrid-SORT [58]	<u>73.0</u>	<u>61.6</u>	94.3	<u>73.3</u>
OA-SORT (Ours)	73.4	62.3	<u>94.4</u>	74.1
<i>*Same Detection:</i>				
ByteTrack [62]	64.1	52.3	95.9	71.4
MixSort-Byte [9]	65.7	54.8	96.2	74.1
OC-SORT [6]	73.7	61.5	96.5	74.0
MixSort-OC [9]	74.1	62.0	96.5	74.4
Hybrid-SORT [58]	<u>74.8</u>	<u>63.2</u>	96.2	<u>75.1</u>
OA-SORT (Ours)	75.2	63.8	<u>96.3</u>	75.8

Table 2. Results on SportsMOT. The same detections are provided by SportsMOT, where * indicates that the detector is trained using the SportsMOT train and validation sets.

Method	HOTA	AssA	MOTA	IDF1
CenterTrack [65]	52.5	51.0	67.8	64.7
FairMOT [61]	59.3	58.0	73.7	72.3
DST-Tracker [5]	60.1	62.1	75.2	72.3
UTM [59]	64.0	62.5	81.8	78.7
DiffusionTrack [33]	60.8	58.8	77.9	73.8
MOTIP [17]	59.2	56.9	75.5	71.2
<i>Same Detection:</i>				
ByteTrack [62]	63.1	62.0	80.3	77.3
OC-SORT [6]	63.2	63.2	78.0	77.5
StrongSORT++ [12]	64.4	64.4	79.6	79.5
PD-SORT [52]	63.9	64.1	79.3	79.2
Hybrid-SORT-REID [58]	64.0	63.5	79.9	78.7
BOT-SORT-REID [1]	65.0	65.5	80.5	80.2
SMILEtrack [53]	65.0	-	80.7	80.1
<i>Integration:</i>				
BOT-SORT [1]	64.6	-	80.6	79.5
OA-BOT (Ours)	65.1	64.8	80.9	79.4
Hybrid-SORT [58]	63.6	63.2	80.6	78.4
OA-SORT (Ours)	64.2	64.0	79.6	79.1

Table 3. Results on MOT17-test with the private detections. The same detection is provided by ByteTrack.

MOT17. Tab. 3 presents the results on MOT17, which represents a more general and typical scenario of linear-motion patterns. OA-SORT still surpasses the baseline, Hybrid-SORT (+0.6 HOTA and +0.7 IDF1), even outperforms Hybrid-SORT-REID by +0.5 AssA and +0.3 IDF1. These results demonstrate that occlusion-awareness is highly versatile across different motion patterns. Moreover, the occlusion-awareness brings benefits for BOT-SORT without ReID (OA-BOT).

Overall, integrating occlusion-awareness into the tracking framework achieves better performance. These results also indicate that the occlusion-aware framework enhances tracking robustness under different occlusion scenarios, involving variable-speed and camera motion, validating the rationality. Even on MOT17, which includes numerous false detections and long-term missed detections, there have been improvements. Additionally, we evaluate Hybrid-SORT on MOT20 [10], achieving an additional +0.4 IDF1 improvement. Notably, optimizing the number of missed and false detections is not the primary focus of this work.

5.3. Ablation Study

Detections and ReID features, provided by Hybrid-SORT [18, 21, 58], are utilized in this section.

Component Ablation. The results for OAO, BAM, and GM are reported in Tab. 4. These results demonstrate that introducing occlusion-awareness significantly improves tracking association and accuracy. Along with integrating OAO, the tracker’s association is enhanced, with

OAO	BAM	GM	ReID	HOTA	AssA	IDF1	T (ms)
				59.4	44.9	60.7	9.57
✓				59.9	45.6	60.9	+1.96
✓		✓		60.6	46.7	62.0	+9.25
✓	✓			60.5	46.5	62.2	+3.81
✓	✓	✓		61.5	48.0	63.7	+14.99
			✓	63.1	50.4	65.1	60.95
✓	✓	✓	✓	63.4	50.8	65.3	+15.32

Table 4. Components ablation on DanceTrack-val; T (ms) indicates average tracking runtime per frame.

improvements of +0.5 HOTA. Secondly, after optimizing KF’s estimate through BAM, the HOTA is significantly improved by +1.1, which has only a minor impact on inference speed (average +3.81ms). Notably, integrating GM brings improvements of +2.1 HOTA. Although GM increases the average tracking time to 24.56 ms per frame, the system still satisfies real-time tracking requirements. Additionally, with the use of occlusion-awareness, Hybrid-SORT-REID also gets benefits. Notably, given X trajectories with Z interactions and N detected objects with M interactions, the computational complexity is approximately: OAM: $\mathcal{O}(X^2 + Z * \hat{A})$ or $\mathcal{O}(N^2 + M * \hat{A})$, OAO: $\mathcal{O}(Z * N)$, and BAM: $\mathcal{O}(M)$, where \hat{A} denotes the average pixel area of the detected bounding boxes.

σ^x and σ^y in GM. Smaller σ^x and σ^y values concentrate the weights more heavily at the center of the bounding box, reducing edge influence. For pedestrian tracking, the optimal parameters may vary according to the motion pattern. For example, the Dancetrack dataset primarily consists of dance scenes, and the change in hand and leg positions introduces a significant amount of background; therefore, the horizontal and vertical weights should be smaller. Experimental results confirm our analysis that $\sigma^x = w/3\sqrt{2}$ and $\sigma^y = h/3$ for DanceTrack can achieve good performance.

GM and τ . A larger τ as defined in Eq. (8) mitigates the position cost confusion due to inaccurate detection caused by occlusion, but is also likely to destroy the spatial consistency expression. Thus, we show Fig. 4 that the tracking performance of OAO and BAM components under different GM and values of $\tau \in [0.1, 0.5]$, which analyzes the influence of different τ for different configurations. Overall, our results agree with our analysis that increasing τ from $\tau = 0.1$ can yield benefits using the tracker with OAO, BAM, and GM on DanceTrack. However, increasing τ beyond a certain value degrades performance due to compromised spatial consistency. Secondly, GM effectively enhances the performance of both OAO and BAM components, regardless of the τ .

Bias-Aware Momentum. To mitigate the impact of inaccurate detections, BAM (Sec. 4.3) combines the spatial-

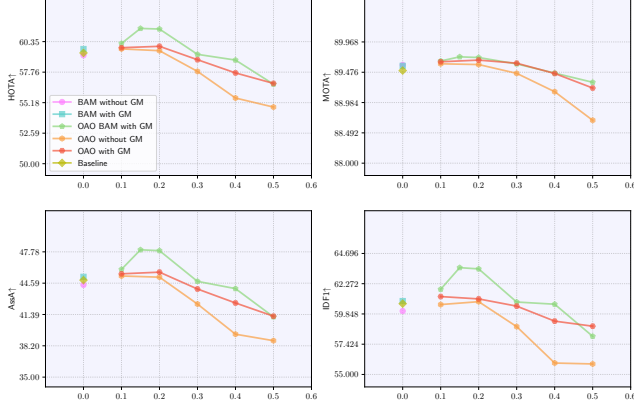


Figure 4. The results under GM and different values of τ .

	HOTA	AssA	IDF1
0.1	60.69	46.78	62.47
0.3	60.99	47.16	62.99
0.4	<u>61.26</u>	<u>47.61</u>	<u>63.00</u>
0.45	61.04	47.27	62.65
0.5	61.02	47.24	62.77
IoU [60]	61.49	48.03	63.65
HMIoU [58]	61.49	48.03	63.65

Table 5. Results on DanceTrack-val with different BAM.

consistency metric [58, 60] and occlusion information. There are alternative configurations, such as using a constant value instead of the spatial consistency metric [58, 60]. The results in Tab. 5 indicate that incorporating the spatial consistency metric [58, 60] for adaptive momentum adjustment achieves better performance. To reduce the extra computation, the spatial consistency metric can follow the tracker. Herein, following Hybrid-SORT [58], OA-SORT utilizes HMIoU.

Application on Other Trackers. We incorporated OAO and BAM with GM into different trackers, and the results are shown in Tab. 6. Consequently, OAO and BAM consistently enhance each tracker’s performance, demonstrating their adaptability and reusability. Notably, the four trackers have different association methods and strategies. The TrackTrack [45] employs additional detections, ReID feature [21], novel allocation method differing from the Hungarian algorithm, and the NSA Kalman Filter [11] that is an extended Kalman filter. Its association process for confirmed trajectory is between OAO and BAM.

5.4. Limitations

Overall, the occlusion-aware framework has stronger robustness in occluded scenes. However, when the lower parts of objects are occluded or when objects are airborne (*e.g.*, jumping), the framework’s association performance

Tracker	Byte	OAO	BAM	HOTA	IDF1
SORT [2]				48.4	49.6
	✓			48.3	50.0
	✓	✓		50.4	53.0
	✓	✓	✓	50.4	53.3
Bytetrack [62]	-	-	-	-	-
	✓			47.1	52.7
	✓	✓		48.8	55.1
	✓	✓	✓	49.3	55.7
OC-SORT [6]	✓			52.3	52.0
	✓	✓		52.4	51.5
	✓	✓		53.6	53.3
	✓	✓	✓	53.8	53.9
TrackTrack [45]	-	-	-	-	-
	✓			59.3	61.1
	✓	✓		59.7	61.7
	✓	✓	✓	59.9	62.0

Table 6. Results on DanceTrack-val. To highlight BAM, the low-score detection association (Byte) is integrated.

decreases compared to the baseline. As shown in Fig. 1, sequence #0026 serves as a representative example. In this case, the bottom-edge-based method struggles to accurately capture the depth relationships, thereby affecting the performance of occlusion-aware framework. Secondly, the occlusion state and its temporal variations are continuous over time. Although this paper reveals that observing and utilizing occlusion state can enhance association robustness, the lack of long-term occlusion modeling leads to instability in association. This issue will be addressed in future research.

6. Conclusion

In this paper, we explore the impact of occlusion on position association. Inaccurate detection and cost confusion caused by occlusion seriously affect tracking accuracy. However, existing trackers have not modeled the occlusion status of bounding box detections. To address this, the proposed occlusion-aware framework integrates occlusion status into the position association and the update phase of KF. Notably, GM is introduced to construct OAM, enabling more accurate evaluation of occlusion severity. Comprehensive experiments conduct on multiple datasets fully validate the importance of integrating occlusion states. In terms of the ablation study, the role, practicality, and reusability of GM, OAO, and BAM are thoroughly demonstrated. In summary, the three plug-and-play, training-free components are easily integrated into existing trackers. In future work, we will explore more robust occlusion state estimation methods and develop low-complexity approaches for estimating occlusion severity.

Acknowledgments

This work was supported in part by National Natural Science Foundation of China (Grant 62302324); in part by Sichuan Province Science and Technology Support Program (Grant 2024NSFSC0500); in part by the Fundamental Research Funds for the Central Universities (Grant YJ202420); in part by Sichuan University young teachers science and technology innovation ability improvement project (Grant 2024SCUQJTX028).

References

- [1] Nir Aharon, Roy Orfaig, and Ben-Zion Bobrovsky. Bot-sort: Robust associations multi-pedestrian tracking. *arXiv preprint arXiv:2206.14651*, 2022. 2, 7
- [2] Alex Bewley, Zongyuan Ge, Lionel Ott, Fabio Ramos, and Ben Uroft. Simple online and realtime tracking. In *2016 IEEE International Conference on Image Processing (ICIP)*, pages 3464–3468, 2016. 1, 2, 5, 6, 8
- [3] Erik Bochinski, Volker Eiselein, and Thomas Sikora. High-speed tracking-by-detection without using image information. In *2017 14th IEEE international conference on advanced video and signal based surveillance (AVSS)*, pages 1–6. IEEE, 2017. 2
- [4] Michael D Breitenstein, Fabian Reichlin, Bastian Leibe, Esther Koller-Meier, and Luc Van Gool. Robust tracking-by-detection using a detector confidence particle filter. In *2009 IEEE 12th International Conference on Computer Vision*, pages 1515–1522. IEEE, 2009. 1
- [5] Jinkun Cao, Hao Wu, and Kris Kitani. Track targets by dense spatio-temporal position encoding. *arXiv preprint arXiv:2210.09455*, 2022. 6, 7
- [6] Jinkun Cao, Jiangmiao Pang, Xinshuo Weng, Rawal Khirrodkar, and Kris Kitani. Observation-centric sort: Rethinking sort for robust multi-object tracking. In *Proceedings of the IEEE/CVF conference on computer vision and pattern recognition*, pages 9686–9696, 2023. 2, 5, 6, 7, 8
- [7] Jieyu Chen, Zhenghao Xi, Junxin Lu, and Jingjing Ji. Multi-object tracking based on network flow model and orb feature. *APPLIED INTELLIGENCE*, 52(11):12282–12300, 2022. 2
- [8] Peng Chu, Jiang Wang, Quanzeng You, Haibin Ling, and Zicheng Liu. Transmot: Spatial-temporal graph transformer for multiple object tracking. In *Proceedings of the IEEE/CVF Winter Conference on applications of computer vision*, pages 4870–4880, 2023. 6
- [9] Yutao Cui, Chenkai Zeng, Xiaoyu Zhao, Yichun Yang, Gangshan Wu, and Limin Wang. Sportsmot: A large multi-object tracking dataset in multiple sports scenes. In *Proceedings of the IEEE/CVF International Conference on Computer Vision*, pages 9921–9931, 2023. 5, 6
- [10] Patrick Dendorfer, Hamid Rezatofighi, Anton Milan, Javen Shi, Daniel Cremers, Ian Reid, Stefan Roth, Konrad Schindler, and Laura Leal-Taixé. Mot20: A benchmark for multi object tracking in crowded scenes. *arXiv preprint arXiv:2003.09003*, 2020. 7, 5
- [11] Yunhao Du, Junfeng Wan, Yanyun Zhao, Binyu Zhang, Zhihang Tong, and Junhao Dong. Giaotracker: A comprehensive framework for mcmot with global information and optimizing strategies in visdrone 2021. In *2021 IEEE/CVF International Conference on Computer Vision Workshops (ICCVW)*, pages 2809–2819, 2021. 1, 2, 8
- [12] Yunhao Du, Zhicheng Zhao, Yang Song, Yanyun Zhao, Fei Su, Tao Gong, and Hongying Meng. Strongsort: Make deepsort great again. *IEEE Transactions on Multimedia*, 2023. 2, 6, 7
- [13] Hao-Shu Fang, Shuqin Xie, Yu-Wing Tai, and Cewu Lu. Rmpe: Regional multi-person pose estimation. In *Proceedings of the IEEE international conference on computer vision*, pages 2334–2343, 2017. 3
- [14] Hao-Shu Fang, Jiefeng Li, Hongyang Tang, Chao Xu, Haoyi Zhu, Yuliang Xiu, Yong-Lu Li, and Cewu Lu. Alphapose: Whole-body regional multi-person pose estimation and tracking in real-time. *IEEE Transactions on Pattern Analysis and Machine Intelligence*, pages 1–17, 2022. 1
- [15] Tobias Fischer, Thomas E. Huang, Jiangmiao Pang, Linlu Qiu, Haofeng Chen, Trevor Darrell, and Fisher Yu. Qdtrack: Quasi-dense similarity learning for appearance-only multiple object tracking. *IEEE Transactions on Pattern Analysis and Machine Intelligence*, 45(12):15380–15393, 2023. 6
- [16] Ruopeng Gao and Limin Wang. MeMOTR: Long-Term Memory-Augmented Transformer for Multi-Object Tracking. In *2023 IEEE/CVF Int. Conf. Comput. Vis. ICCV*, pages 9867–9876, Paris, France, 2023. IEEE. 6
- [17] Ruopeng Gao, Ji Qi, and Limin Wang. Multiple object tracking as id prediction. In *Proceedings of the Computer Vision and Pattern Recognition Conference*, pages 27883–27893, 2025. 6, 7
- [18] Zheng Ge, Songtao Liu, Feng Wang, Zeming Li, and Jian Sun. Yolox: Exceeding yolo series in 2021. *arXiv preprint arXiv:2107.08430*, 2021. 7
- [19] Shoudong Han, Piao Huang, Hongwei Wang, En Yu, Donghaisheng Liu, and Xiaofeng Pan. Mat: Motion-aware multi-object tracking. *Neurocomputing*, 476:75–86, 2022. 2
- [20] Xudong Han, Nobuyuki Oishi, Yueying Tian, Elif Ucurum, Rupert Young, Chris Chatwin, and Philip Birch. Ettrack: enhanced temporal motion predictor for multi-object tracking. *Applied Intelligence*, 55(1):1–17, 2025. 6
- [21] Lingxiao He, Xingyu Liao, Wu Liu, Xinchun Liu, Peng Cheng, and Tao Mei. Fastreid: A pytorch toolbox for general instance re-identification. In *Proceedings of the 31st ACM International Conference on Multimedia*, pages 9664–9667, 2023. 2, 7, 8
- [22] Hou-Ning Hu, Yung-Hsu Yang, Tobias Fischer, Trevor Darrell, Fisher Yu, and Min Sun. Monocular quasi-dense 3d object tracking. *IEEE Transactions on Pattern Analysis and Machine Intelligence*, pages 1–1, 2022. 1
- [23] Simon J Julier and Jeffrey K Uhlmann. New extension of the kalman filter to nonlinear systems. In *Signal processing, sensor fusion, and target recognition VI*, pages 182–193. Spie, 1997. 2
- [24] Rudolf Emil Kalman et al. Contributions to the theory of optimal control. *Bol. soc. mat. mexicana*, 5(2):102–119, 1960. 1

- [25] Donghwa Kang, Seunghoon Lee, Hoon Sung Chwa, Seung-Hwan Bae, Chang Mook Kang, Jinkyu Lee, and Hyeong-boo Baek. Rt-mot: Confidence-aware real-time scheduling framework for multi-object tracking tasks. In *2022 IEEE Real-Time Systems Symposium (RTSS)*, pages 318–330. IEEE, 2022. 2
- [26] B. Keni and S. Rainer. Evaluating multiple object tracking performance: The clear mot metrics. *Eurasip Journal on Image & Video Processing*, 2008(1):246309, 2008. 5
- [27] Taeklim Kim and Tae-Hyoung Park. Extended kalman filter (ekf) design for vehicle position tracking using reliability function of radar and lidar. *Sensors*, 20(15):4126, 2020. 2
- [28] Harold W Kuhn. The hungarian method for the assignment problem. *Naval research logistics quarterly*, 2(1-2):83–97, 1955. 1
- [29] Chao Liang, Zhipeng Zhang, Xue Zhou, Bing Li, Shuyuan Zhu, and Weiming Hu. Rethinking the competition between detection and reid in multiobject tracking. *IEEE Transactions on Image Processing*, 31:3182–3196, 2022. 6
- [30] Tsung-Yi Lin, Piotr Dollár, Ross Girshick, Kaiming He, Bharath Hariharan, and Serge Belongie. Feature pyramid networks for object detection. In *Proceedings of the IEEE conference on computer vision and pattern recognition*, pages 2117–2125, 2017. 2
- [31] Zelin Liu, Xinggong Wang, Cheng Wang, Wenyu Liu, and Xiang Bai. Sparsetrack: Multi-object tracking by performing scene decomposition based on pseudo-depth. *IEEE Transactions on Circuits and Systems for Video Technology*, 2025. 2, 4, 5, 6
- [32] Jonathon Luiten, Aljosa Osep, Patrick Dendorfer, Philip Torr, Andreas Geiger, Laura Leal-Taixé, and Bastian Leibe. Hota: A higher order metric for evaluating multi-object tracking. *International Journal of Computer Vision*, pages 1–31, 2020. 5
- [33] Run Luo, Zikai Song, Lintao Ma, Jinlin Wei, Wei Yang, and Min Yang. Diffusiontrack: Diffusion model for multi-object tracking. In *Proceedings of the AAAI conference on artificial intelligence*, pages 3991–3999, 2024. 6, 7
- [34] Wenhan Luo, Junliang Xing, Anton Milan, Xiaoqin Zhang, Wei Liu, and Tae-Kyun Kim. Multiple object tracking: A literature review. *Artificial Intelligence*, 293:103448, 2021. 1
- [35] Weiyi Lv, Yuhang Huang, Ning Zhang, Rwei-Sung Lin, Mei Han, and Dan Zeng. Diffmot: A real-time diffusion-based multiple object tracker with non-linear prediction. In *Proceedings of the IEEE/CVF Conference on Computer Vision and Pattern Recognition*, pages 19321–19330, 2024. 6
- [36] Jiaqi Ma, Jinfu Yang, Jiahui Zhang, and Fuji Fu. Online multiple object tracker with enhanced features. *Journal of Electronic Imaging*, 32(1):013030, 2023. 2
- [37] Gerard Maggolino, Adnan Ahmad, Jinkun Cao, and Kris Kitani. Deep oc-sort: Multi-pedestrian tracking by adaptive re-identification. In *2023 IEEE International Conference on Image Processing (ICIP)*, pages 3025–3029. IEEE, 2023. 2, 4
- [38] Mehdi Miah, Guillaume-Alexandre Bilodeau, and Nicolas Saunier. Learning data association for multi-object tracking using only coordinates. *Pattern Recognition*, 160:111169, 2025. 6
- [39] Anton Milan, Laura Leal-Taixé, Ian D. Reid, Stefan Roth, and Konrad Schindler. MOT16: A benchmark for multi-object tracking. *CoRR*, abs/1603.00831, 2016. 5
- [40] Zheng Qin, Sanping Zhou, Le Wang, Jinghai Duan, Gang Hua, and Wei Tang. Motiontrack: Learning robust short-term and long-term motions for multi-object tracking. In *Proceedings of the IEEE/CVF Conference on Computer Vision and Pattern Recognition*, pages 17939–17948, 2023. 2
- [41] Kha Gia Quach, Pha Nguyen, Chi Nhan Duong, Tien Dai Bui, and Khoa Luu. Depth perspective-aware multiple object tracking. In *Engineering Applications of AI and Swarm Intelligence*, pages 181–205. Springer, 2024. 4
- [42] Hao Ren, Shoudong Han, Huilin Ding, Ziwen Zhang, Hongwei Wang, and Faquan Wang. Focus on details: Online multi-object tracking with diverse fine-grained representation. In *Proceedings of the IEEE/CVF conference on computer vision and pattern recognition*, pages 11289–11298, 2023. 6
- [43] Ergys Ristani, Francesco Solera, Roger Zou, Rita Cucchiara, and Carlo Tomasi. Performance measures and a data set for multi-target, multi-camera tracking. In *COMPUTER VISION - ECCV 2016 WORKSHOPS, PT II*, pages 17–35, 2016. 14th European Conference on Computer Vision (ECCV), Amsterdam, NETHERLANDS, OCT 08-16, 2016. 5
- [44] Jenny Seidenschwarz, Guillem Brasó, Victor Castro Serrano, Ismail Elezi, and Laura Leal-Taixé. Simple cues lead to a strong multi-object tracker. In *Proceedings of the IEEE/CVF conference on computer vision and pattern recognition*, pages 13813–13823, 2023. 6
- [45] Kyujin Shim, Kangwook Ko, Yujin Yang, and Changick Kim. Focusing on tracks for online multi-object tracking. In *Proceedings of the Computer Vision and Pattern Recognition Conference*, pages 11687–11696, 2025. 2, 5, 8, 3
- [46] Daniel Stadler and Jurgen Beyerer. Improving multiple pedestrian tracking by track management and occlusion handling. In *Proceedings of the IEEE/CVF conference on computer vision and pattern recognition*, pages 10958–10967, 2021. 2
- [47] Peize Sun, Jinkun Cao, Yi Jiang, Rufeng Zhang, Enze Xie, Zehuan Yuan, Changhu Wang, and Ping Luo. Transtrack: Multiple object tracking with transformer. *arXiv preprint arXiv:2012.15460*, 2020. 6
- [48] Peize Sun, Jinkun Cao, Yi Jiang, Zehuan Yuan, Song Bai, Kris Kitani, and Ping Luo. Dancetrack: Multi-object tracking in uniform appearance and diverse motion. *CoRR*, abs/2111.14690, 2021. 5
- [49] Zhihong Sun, Jun Chen, Mithun Mukherjee, Chao Liang, Weijian Ruan, and Zhigeng Pan. Online multiple object tracking based on fusing global and partial features. *Neurocomputing*, 470:190–203, 2022. 3
- [50] Ashish Vaswani, Noam Shazeer, Niki Parmar, Jakob Uszkoreit, Llion Jones, Aidan N Gomez, Łukasz Kaiser, and Illia Polosukhin. Attention is all you need. *Advances in neural information processing systems*, 30, 2017. 2

- [51] Balaji Veeramani, John W Raymond, and Pritam Chanda. Deepsort: deep convolutional networks for sorting haploid maize seeds. *BMC bioinformatics*, 19(9):1–9, 2018. 2
- [52] Yanchao Wang, Dawei Zhang, Run Li, Zhonglong Zheng, and Minglu Li. Pd-sort: Occlusion-robust multi-object tracking using pseudo-depth cues. *IEEE Transactions on Consumer Electronics*, 2025. 1, 2, 4, 5, 6, 7
- [53] Yu-Hsiang Wang, Jun-Wei Hsieh, Ping-Yang Chen, Ming-Ching Chang, Hung-Hin So, and Xin Li. Smiletrack: Similarity learning for occlusion-aware multiple object tracking. In *Proceedings of the AAAI conference on artificial intelligence*, pages 5740–5748, 2024. 7
- [54] Zhongdao Wang, Liang Zheng, Yixuan Liu, Yali Li, and Shengjin Wang. Towards real-time multi-object tracking. In *European Conference on Computer Vision*, pages 107–122. Springer, 2020. 2
- [55] Changcheng Xiao, Qiong Cao, Zhigang Luo, and Long Lan. Mambatrack: a simple baseline for multiple object tracking with state space model. In *Proceedings of the 32nd ACM International Conference on Multimedia*, pages 4082–4091, 2024. 6
- [56] Changcheng Xiao, Qiong Cao, Yujie Zhong, Long Lan, Xiang Zhang, Zhigang Luo, and Dacheng Tao. Motiontrack: Learning motion predictor for multiple object tracking. *Neural Networks*, 179:106539, 2024. 6
- [57] Fan Yang, Shigeyuki Odashima, Shoichi Masui, and Shan Jiang. Hard to track objects with irregular motions and similar appearances? make it easier by buffering the matching space. In *Proceedings of the IEEE/CVF winter conference on applications of computer vision*, pages 4799–4808, 2023. 6
- [58] Mingzhan Yang, Guangxin Han, Bin Yan, Wenhua Zhang, Jinqing Qi, Huchuan Lu, and Dong Wang. Hybrid-sort: Weak cues matter for online multi-object tracking. In *Proceedings of the AAAI Conference on Artificial Intelligence*, pages 6504–6512, 2024. 1, 2, 5, 6, 7, 8, 3
- [59] Sisi You, Hantao Yao, Bing-Kun Bao, and Changsheng Xu. Utm: A unified multiple object tracking model with identity-aware feature enhancement. In *Proceedings of the IEEE/CVF Conference on Computer Vision and Pattern Recognition*, pages 21876–21886, 2023. 7, 6
- [60] Jiahui Yu, Yuning Jiang, Zhangyang Wang, Zhimin Cao, and Thomas Huang. Unitbox: An advanced object detection network. In *Proceedings of the 24th ACM international conference on Multimedia*, pages 516–520, 2016. 1, 5, 8
- [61] Yifu Zhang, Chunyu Wang, Xinggang Wang, Wenjun Zeng, and Wenyu Liu. Fairmot: On the fairness of detection and re-identification in multiple object tracking. *International Journal of Computer Vision*, 129(11):3069–3087, 2021. 2, 6, 7
- [62] Yifu Zhang, Peize Sun, Yi Jiang, Dongdong Yu, Fucheng Weng, Zehuan Yuan, Ping Luo, Wenyu Liu, and Xinggang Wang. Bytetrack: Multi-object tracking by associating every detection box. In *European Conference on Computer Vision*, pages 1–21. Springer, 2022. 1, 2, 5, 6, 7, 8, 3
- [63] Yukuan Zhang, Housheng Xie, Yunhua Jia, Jingrui Meng, Meng Sang, Junhui Qiu, Shan Zhao, and Yang Yang. Aipt: Adaptive information perception for online multi-object tracking. *Knowledge-Based Systems*, 285:111369, 2024. 6
- [64] Liang Zheng, Yi Yang, and Alexander G Hauptmann. Person re-identification: Past, present and future. *arXiv preprint arXiv:1610.02984*, 2016. 2
- [65] Xingyi Zhou, Vladlen Koltun, and Philipp Krähenbühl. Tracking objects as points. In *Computer Vision – ECCV 2020*, pages 474–490, Cham, 2020. Springer International Publishing. 2, 6, 7
- [66] Zongwei Zhou, Wenhan Luo, Qiang Wang, Junliang Xing, and Weiming Hu. Distractor-aware discrimination learning for online multiple object tracking. *Pattern Recognition*, 107:107512, 2020. 2
- [67] Tianyu Zhu, Markus Hiller, Mahsa Ehsanpour, Rongkai Ma, Tom Drummond, Ian Reid, and Hamid Rezaatoughi. Looking beyond two frames: End-to-end multi-object tracking using spatial and temporal transformers. *IEEE Transactions on Pattern Analysis and Machine Intelligence*, 45(11):12783–12797, 2023. 2
- [68] Songshang Zou, Hao Chen, Hui Feng, Guangyi Xiao, Zhen Qin, and Weiwei Cai. Traffic flow video image recognition and analysis based on multi-target tracking algorithm and deep learning. *IEEE Transactions on Intelligent Transportation Systems*, pages 1–14, 2022. 1
- [69] Zhibo Zou, Junjie Huang, and Ping Luo. Compensation tracker: reprocessing lost object for multi-object tracking. In *Proceedings of the IEEE/CVF winter conference on applications of computer vision*, pages 307–317, 2022. 2

Occlusion-Aware SORT: Observing Occlusion for Robust Multi-Object Tracking

Supplementary Material

7. Reliability Analysis and Pseudo code

7.1. Occlusion-Aware Module

7.1.1. Reliability Analysis

Occlusion in 2D image space follows two primary spatial cues:

- Depth ordering: In pedestrian or vehicle scenes, 2D overlap typically indicates physical proximity, and bounding boxes with significantly lower bottom-edge y-coordinates (*i.e.*, larger b , Fig. 3) are typically nearer to the camera and thus more likely to occlude others.
- Intersection area: For objects with intersecting bounding boxes (non-zero IoU), the overlapping region correlates with the extent of physical occlusion.

OAM leverages both cues and constructs a logical occlusion relationship matrix:

$$C_{IoU}(\mathcal{D}_i, \mathcal{D}_j) > 0 \wedge b_j - b_i > thre_{occ} \quad (12)$$

where $C_{IoU}(\mathcal{D}_i, \mathcal{D}_j)$ ensures that only **geometrically consistent occlusion hypotheses** are considered; $thre_{occ}$ aims to reduce **false depth ordering brought by fluctuations and strong competition at the bottom edge**.

In terms of GM (Eq. (5)), for each bounding box i , σ_i^x and σ_i^y are defined by:

$$\sigma_i^x = \frac{w_i}{k_x}, \quad \sigma_i^y = \frac{h_i}{k_y}. \quad (13)$$

The GM aims to reflect the relative importance of pixels affected by occlusion. All in all, OAM applies a soft probabilistic prior that reflects the confidence that multiple trajectories should be associated. This design complements hard IoU logic from the trajectory view, emphasizing the association of unoccluded trajectories.

7.1.2. Pseudocode

$\mathcal{D} = [l, t, r, b]$ indicates detected bounding boxes, where l, t, r, b denote the left, top, right, and bottom of the bounding box. Herein, we assume that N bounding boxes ($\mathcal{D} \in \mathbb{R}^{*N \times 4}$), need to be associated with high-score detections, where the width and height of the image are W and H . The Pseudo-code about OAM is shown as follows, where \leftarrow indicates assignment. Algorithm 1 implements three key components:

- Lines 5-9: Eq. (5);
- Lines 10-35: Eq. (2) and Eq. (4);
- To improve computational efficiency, lines 2-3 and line 6 are used for data filtering.

Moreover, it is worth noting that to avoid fluctuations in estimation or detection, we set a threshold ($thre_{occ}$) for comparing the bottom edges (line 12 of the algorithm). When the difference value exceeds $thre_{occ}$, it will be considered an occlusion. The $thre_{occ}$ for the experiment in our work is 5. This can also alleviate the corresponding issues caused by incorrect bottom-edge depth ordering. Moreover, Gaussian scaling factors k_x and k_y are used to adapt to the proportion of background pixels within each detected bounding box. Their values are discussed in the Sec. 8.1.

7.2. Occlusion-Aware Offset

7.2.1. Reliability Analysis

Occlusion-Aware Offset (OAO) addresses the limitation of traditional IoU-based association in occluded scenarios, and this situation is analyzed in Sec. 3. Under occlusion, the spatial relationship between detections and tracks becomes unreliable due to:

- **Unreliable prediction of lost trajectory:** Multiple trajectories competing for the same detection region due to overlapping occlusions, as shown in Fig. 8 (in Sec. 8.5).
- **Positional ambiguity:** Occluded objects experience centroid shifts, bounding box distortions or strong competition, making IoU an inconsistent measure of true spatial proximity. This situation leads to cost confusion between detected bounding box and trajectories, causing ID switch as shown in Fig. 9 (in Sec. 8.5).

OAO mitigates these issues by incorporating occlusion awareness into the association cost matrix from the view of trajectory, effectively enhancing the discriminative power of the cost.

7.2.2. Pseudocode

We assume that the N detections $\mathcal{D} \in \mathbb{R}^{N \times 4}$ need to be associated with M estimations \mathbf{X} . The pseudo-code for Occlusion-Aware Offset (OAO) is shown Algorithm 2. The spatial consistency score about detections and estimations will be updated. Notably, the initial calculations of the spatial consistency score are different in different trackers. For example, Hybrid-SORT [58] uses $HMIoU$; PD-SORT [52] uses $DVIoU$ that is a 3D IoU. Herein, C_{IoU} and IoU are used uniformly.

7.3. Bias-Aware Momentum

7.3.1. Reliability Analysis

In theory, occlusion-aware tracking requires dynamic adjustment of both the process noise \mathbf{Q} and measurement noise \mathbf{R} . However, real-time estimation of these parameters presents significant challenges:

Algorithm 1 Occlusion-Aware Module ($\hat{O}c \leftarrow OAM(\cdot)$)

Input: Detected bounding boxes $\mathcal{D} \in \mathbb{R}^{N \times 4}$ **Parameter:** Image dimensions (W, H), Gaussian scaling factors k_x, k_y , occlusion trigger threshold $thre_{occ}$ **Output:** Refined occlusion coefficients $\hat{O}c \in \mathbb{R}^N$

```
1: Initialize  $\hat{O}c \leftarrow \mathbf{0}^N$  {Initialize occlusion coefficients}
2:  $IoU_{\mathcal{D}} \in \mathbb{R}^{N \times N} \leftarrow C_{IoU}(\mathcal{D}, \mathcal{D})$  {Compute IoU matrix}
3:  $\text{diag}(IoU_{\mathcal{D}}) \leftarrow 0$  {Ignore self-relation}
# -----Spatial consistency determination-----
4: if  $\max(IoU_{\mathcal{D}}) > 0$  then
5:    $GM \in \mathbb{R}^{H \times W} \leftarrow \mathbf{0}^{H \times W}$  {Initialize Gauss-Map}
6:   for each  $\mathcal{D}_i$  in  $\{\mathcal{D}_i | \max(IoU_{\mathcal{D}}[i]) > 0\}$  do
7:      $\sigma_i^x \leftarrow w_i/k_x, \sigma_i^y \leftarrow h_i/k_y$  {Adaptive sigmas}
8:      $GM[t_i : b_i, l_i : r_i] \leftarrow \max(GM[t_i : b_i, l_i : r_i], \text{drawGaussian}(\mathcal{D}_i, \sigma_i^x, \sigma_i^y))$ 
9:   end for
10:   $\text{bottoms} \leftarrow \mathcal{D}[:, 3]$  {Bottom y-coordinates ( $b$ )}
11:   $\text{areas} \leftarrow (\mathcal{D}[:, 2] - \mathcal{D}[:, 0]) \times (\mathcal{D}[:, 3] - \mathcal{D}[:, 1])$  {Calculate Bounding-box areas}
12:   $\text{validMask} \leftarrow (\text{bottoms}[:, \text{None}] - \text{bottoms}[\text{None}, :]) \leq -thre_{occ} \wedge (IoU_{\mathcal{D}} > 0)$  {The occlusion relationship matrix.}
13:   $\text{all}_L, \text{all}_T, \text{all}_R, \text{all}_B \leftarrow \mathcal{D}$  {Vectorized coordinates}
# -----Obtaining occlusion coefficient-----
14:  for each  $\mathcal{D}_i$  and  $i$  in  $\mathcal{D}$  do
15:     $js \leftarrow \{j | \text{validMask}[i, j] = \text{TRUE}\}$  {Select objects that occludes object  $i$ .}
16:    if  $js = \emptyset$  then
17:      continue
18:    end if
19:     $l_i, t_i, r_i, b_i \leftarrow \mathcal{D}_i$ 
20:     $\text{localGM} \in \mathbb{R}^{h_i \times w_i} \leftarrow GM[t_i : b_i, l_i : r_i]$  {Crop local GM from  $GM$ : Gaussian heatmap about  $\mathcal{D}_i$ }
21:     $T \in \mathbb{R}^{\text{len}(js)} \leftarrow \max(t_i, \text{all}_T[js])$  { $\text{len}(js)$  is array length of  $js$ }
22:     $B \in \mathbb{R}^{\text{len}(js)} \leftarrow \min(b_i, \text{all}_B[js])$ 
23:     $L \in \mathbb{R}^{\text{len}(js)} \leftarrow \max(l_i, \text{all}_L[js])$ 
24:     $R \in \mathbb{R}^{\text{len}(js)} \leftarrow \min(r_i, \text{all}_R[js])$ 
25:     $tClip \in \mathbb{R}^{\text{len}(js)} \leftarrow \max(0, T - t_i)$  {Coordinate transformation}
26:     $bClip \in \mathbb{R}^{\text{len}(js)} \leftarrow \min(h_i, B - b_i)$ 
27:     $lClip \in \mathbb{R}^{\text{len}(js)} \leftarrow \max(0, L - l_i)$ 
28:     $rClip \in \mathbb{R}^{\text{len}(js)} \leftarrow \min(w_i, R - r_i)$ 
29:     $\text{occlusionMap} \leftarrow \mathbf{0}^{h_i \times w_i}$  {Boolean occlusion map: occlusion region}
30:    for each  $j$  in  $js$  do
31:       $\text{occlusionMap}[tClip[j] : bClip[j], lClip[j] : rClip[j]] \leftarrow 1$  {Obtain the overlapping region}
32:    end for
33:     $\hat{O}c_i \leftarrow \frac{\sum(\text{localGM} \odot \text{occlusionMap})}{\text{areas}_i}$  { $\odot$  indicates Hadamard (element-wise) product.}
34:  end for
35: end if
36: return  $\hat{O}c$ 
```

Algorithm 2 Occlusion-Aware Offset

 $S \leftarrow OAO(\mathbf{X}, IoU_{\mathcal{D}, \mathbf{X}})$ **Input:** estimations $\mathbf{X} \in \mathbb{R}^{M \times 4}$ from tracked trajectories; $IoU_{\mathcal{D}, \mathbf{X}} \in \mathbb{R}^{N \times M}$ between \mathcal{D} and \mathbf{X} **Parameter:** Coefficient τ that is used to balance IoU and $\hat{O}c$ **Output:** Spatial consistency S

```
1:  $\hat{O}c^{\mathbf{X}} \in \mathbb{R}^{1 \times M} \leftarrow OAM(\mathbf{X})$ 
2:  $S \in \mathbb{R}^{N \times M} \leftarrow \tau \cdot (1 - \hat{O}c^{\mathbf{X}})[\text{None}, :] + (1 - \tau) \cdot IoU_{\mathcal{D}, \mathbf{X}}$  {This describes Eq. (8).}
3: return  $S$ 
```

Refine \mathbf{K}	Dataset	MOTA	HOTA	AssA	IDF1
✓	DanceTrack	89.73	61.49	48.03	63.65
		89.75	60.81	46.96	62.74
✓	MOT17	76.29	67.06	68.74	78.19
		76.11	66.98	68.67	77.74

Table 7. The influence of refining \mathbf{K} through BAM (OA-SORT).

- **Measurement noise estimation:** The error variance of the detection model under varying occlusion intensities is difficult to characterize. Occlusion-induced errors—including feature confusion and information loss—are varied and difficult to model accurately.
- **Process noise estimation:** Motion model errors stem from natural scene dynamics and model residuals, which are inherently unobservable without ground truth. Furthermore, MOT in 2D images involves discrete observations of inherently nonlinear and irregular target motions. Any predictor necessarily exhibits lag during motion transitions, representing an unavoidable inherent error.

Herein, the additional experiments for BAM are conducted, as shown in Tab. 7, for Kalman gain (\mathbf{K}) that can reflect and consider \mathbf{Q} and \mathbf{R} .

The result shows that BAM implements an instantaneous and implicit measurement reliability adjustment for low-confidence detections by directly modifying observation. This approach attempts to regulate the influence of new observations during the update step, eliminating the need for explicit error modeling or covariance recomputation—aligning well with both practical constraints and robustness objectives in real-world MOT. According to Eq. (10) and Eq. (11), the state update in Eq. (11) can be reformulated as:

$$\mathbf{X}_{t|t} = \mathbf{X}_{t|t-1} + \text{BAM} \cdot \mathbf{K}_t (\mathbf{Z}_t - \mathbf{H}_t \mathbf{X}_{t|t-1}). \quad (14)$$

7.3.2. Pseudocode

We assume that a trajectory is association with a low-score detection, $d \in \mathbb{R}^4$; the trajectory’s estimation $\mathbf{x}_{t|t-1} \in \mathbb{R}^4$.

Algorithm 3 Bias-Aware Momentum ($\mathbf{x}_{t|t} = \text{BAM}(d, \mathbf{x}_{t|t-1}, \hat{O}c^z$)

Input: det that is detected bounding box; $\mathbf{x}_{t|t-1}$; $\hat{O}c^z$
Output: Optimized $\mathbf{x}_{t|t}$

- 1: $IoU_{det, \mathbf{x}_{t|t-1}} \in (0, 1] \leftarrow C_{IoU}(det, \mathbf{x}_{t|t-1})$
- 2: $BAM \leftarrow IoU_{det, \mathbf{x}_{t|t-1}} \cdot (1 - \hat{O}c^z)$ {This describes Eq. (9).}
- 3: $z' \leftarrow det$ { z' denotes observations.}
- 4: $\mathbf{x}_{t|t} \leftarrow \mathbf{x}_{t|t-1} + BAM \cdot \mathbf{K}_t(z' - \mathbf{H}_t \mathbf{x}_{t|t-1})$ {We omit unrelated Kalman filtering details for brevity. This describes Eq. (10) and Eq. (11).}
- 5: **return** $\mathbf{x}_{t|t}$

Algorithm 4 Association approach - high-score detections association

{This step can be mixed with the low-score association, such as TrackTrack [45]}

Input: $\mathcal{D}^{high}, \mathcal{T}$

- 1: $\mathcal{E} \leftarrow [t.estimation \text{ in } t \text{ for } \mathcal{T}]$ { \mathcal{E} indicate the estimation of trajectories.}
- 2: $IoU_{\mathcal{D}^{high}, \mathcal{E}} \leftarrow C_{IoU}(\mathcal{D}^{high}, \mathcal{E})$
- 3: $S \leftarrow OAO(\mathcal{E}, IoU_{\mathcal{D}^{high}, \mathcal{E}})$ {This describes Sec. 4.2.}
- 4: $S \leftarrow S + Other_{score}$ {Herein, other scores ($Other_{score}$) are used for allocation besides IoU. For example, Hybrid-SORT [58] and ByteTrack [62] use direction score and detection score. If using other scores, please calculate based on S . That's right here. Notably, this step can be mixed with the third line.}
- 5: $high_Match_{det}, high_Match_{tra} \leftarrow$ the Hungarian Algorithm uses S to allocation

OAM is used on the process of updating combing with the occlusion coefficient of the latest observation $\hat{O}c^z$ of the trajectory. The pseudocode is shown in Algorithm 3.

7.4. Association approach

Given detections \mathcal{D} , trajectories \mathcal{T} , the Pseudo-codes for high-score detections \mathcal{D}^{high} , low-score detections \mathcal{D}^{low} associations, and trajectory updating are shown as Algorithm 4 and Algorithm 5, where $\mathcal{D}^{high} \cup \mathcal{D}^{low} = \mathcal{D}$ and $\mathcal{D}^{high} \cap \mathcal{D}^{low} = \emptyset$.

8. Additional Experiments

8.1. σ^x and σ^y in GM

For object i , σ_i^x and σ_i^y in GM can be indicated as $\frac{w_i}{k_x}$ and $\frac{h_i}{k_y}$. The performance results for different k_x and k_y values are presented as shown in Tab. 8, Tab. 9 and Tab. 10, where the rows represent the same k_x value and the columns represent the same k_y value. As a result, the $(k_x, k_y) = (5, 3)$

Algorithm 5 Association approach - low-score detections association and trajectory updating

Input: $\mathcal{D}^{low}, \mathcal{T}^{un} \in \mathcal{T}$

- 1: $\mathcal{E}^{un} \leftarrow [t.estimation \text{ in } t \text{ for } \mathcal{T}^{un}]$ { \mathcal{E}^{un} indicate the estimation of unmatched trajectories.}
- 2: $IoU_{\mathcal{D}^{low}, \mathcal{E}^{un}} \leftarrow C_{IoU}(\mathcal{D}^{low}, \mathcal{E}^{un})$
- 3: $S \leftarrow IoU_{\mathcal{D}^{low}, \mathcal{E}^{un}} + Other_{score}$ {Herein, other scores ($Other_{score}$) used for allocation besides IoU. For example, Hybrid-SORT [58] and ByteTrack [62] use direction score and detection score. If using other scores, please calculate based on S . That's right here.}
- 4: $Low_Match_{det}, Low_Match_{tra} \leftarrow$ the Hungarian Algorithm uses S to allocation {Store index in \mathcal{D} and \mathcal{T} of matched detections and trajectories.}
- 5: $Match_{det} \leftarrow high_Match_{det} + Low_Match_{det}, Match_{tra} \leftarrow high_Match_{tra} + Low_Match_{tra}$ {If other matches exist, they are merged accordingly.}
- # **Trajectory updating**
- 6: **for** each d, t in $Match_{det}, Match_{tra}$ **do**
- 7: **if** $\mathcal{D}[d]$ is in \mathcal{D}^{low} **then**
- 8: $offset \leftarrow BAM(\mathcal{D}[d], \mathcal{E}[t], \mathcal{T}[t].\hat{O}c)$ { BAM is for \mathcal{D}^{low} . This describes Eq. (10).}
- 9: **else**
- 10: $offset \leftarrow 1$
- 11: **end if**
- 12: $\mathcal{T}[t] \leftarrow$ update $\mathcal{T}[t]$ using $offset$ and $\mathcal{D}[d]$
- 13: **end for**
- 14: $\mathbf{Z} \leftarrow [t.last_observation \text{ for } t \text{ in } \mathcal{T}[Match_{tra}]]$
- 15: $\hat{O}c^z \leftarrow OAM(\mathbf{Z})$
- 16: $[\mathcal{T}[t].\hat{O}c \leftarrow \hat{O}c[t]$ for $\hat{O}c^z[t]$ in $\hat{O}c^z$]

	2	3	4	5	6
2	60.357	60.477	60.366	60.49	60.836
3	60.543	60.699	60.773	61.076	60.979
4	60.682	61.295	61.117	61.003	60.899
5	61.451	61.667	60.965	60.819	60.607
6	61.415	61.035	60.754	60.249	60.391

Table 8. HOTA (%) on the DanceTrack validation set under different (k_x, k_y) .

can achieve the best performance, i.e., $\sigma_i^x = \frac{w_i}{5}$ and $\sigma_i^y = \frac{h_i}{3}$.

The result primarily shows the approximate global optimum on the DanceTrack validation set. However, when k_x or k_y is larger, the Gaussian distribution might be prone to disorder as shown in Fig. 5. To avoid particularity of k_x and k_y , we attempted to reduce $k_x : k_y = 3 * \sqrt{2} : 3 = 1.414 : 1$, because the quadratic term $(\sigma_n^x)^2$ in Eq. (5) as well as $k_x \in (4, 5)$. The results in Tab. 11 agree with us that the

	2	3	4	5	6
2	46.171	46.326	46.268	46.351	47.023
3	46.494	46.794	46.902	47.374	47.363
4	46.732	47.731	47.418	47.318	47.167
5	47.932	48.257	47.211	47.074	46.719
6	47.926	47.379	47.022	46.207	46.472

Table 9. AssA (%) in DanceTrack under different k_x, k_y .

	2	3	4	5	6
2	61.712	61.848	62.176	62.249	62.924
3	62.031	62.312	62.83	63.348	63.037
4	62.198	63.373	63.182	63.069	62.818
5	63.444	63.789	63.074	62.778	62.507
6	63.38	62.943	62.682	61.938	62.292

Table 10. IDF1 (%) in DanceTrack under different k_x, k_y .

Dataset	(k_x, k_y)	HOTA	AssA	IDF1
test	-	62.20	47.40	63.00
	$(3 * \sqrt{2}, 3)$	63.13	48.53	64.17
	$(5, 3)$	62.93	48.23	64.23
val	-	59.39	44.90	60.67
	$(3 * \sqrt{2}, 3)$	61.49	48.03	63.65
	$(5, 3)$	61.67	48.26	63.79
Average	-	60.80	46.15	61.84
	$(3 * \sqrt{2}, 3)$	62.31	48.28	63.91
	$(5, 3)$	62.30	48.25	64.01

Table 11. The performance of OA-SORT under different k_x in DanceTrack. '-' indicates baseline Hybrid-SORT.

performance is better in the DanceTrack test dataset when $k_x = (3 * \sqrt{2}, 3)$. Finally, σ_n^x and σ_n^y are set to $\frac{w_n}{3 * \sqrt{2}}$ and $\frac{y_n}{3}$, respectively.

8.2. Ablation Study for MOT17

The additional ablations for MOT17 are executed as shown in Tab. 12. The results exhibit the performance improvement from different detection, including YOLOX and Public detection (FRCNN) provided by Hybrid-SORT and host, respectively. Overall, in Public detection with lower detection quality, the occlusion-aware framework can still ensure the performance. However, the benefits it brings are not as good as those from high-quality detection. This is due to missed detections and false positives as shown in Fig. 6, which are not the focus of the occlusion-aware framework.

Finally, the camera-motion compensation (CMC [37]) is integrated into OA-SORT under the detection provided by Hybrid-SORT. The results are reported in Tab. 13. Comparing enhancement brought by occlusion-awareness with

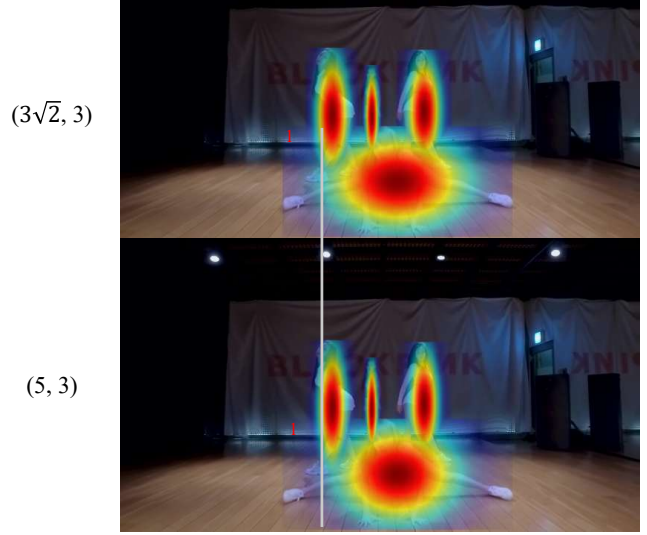
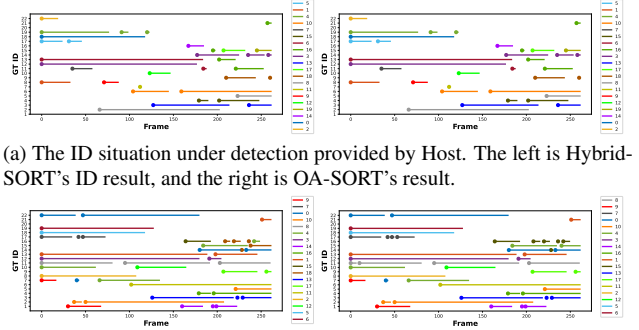


Figure 5. The example about different (k_x, k_y) .

Detection	Method	MOTA	HOTA	AssA	IDF1
YOLOX	Hybrid-SORT	75.65	66.75	68.36	77.64
	OA-SORT	76.29	67.06	68.74	78.19
Public	Hybrid-SORT	46.55	50.16	59.49	56.89
	OA-SORT	46.64	50.22	59.54	57.04

Table 12. Ablation under different detection on MOT17-val.



(a) The ID situation under detection provided by Host. The left is Hybrid-SORT's ID result, and the right is OA-SORT's result.

(b) The ID situation under detection provided by Hybrid-SORT. The left is Hybrid-SORT's ID result, and the right is OA-SORT's result.

Figure 6. The results on MOT17-09. The different color indicates different trajectory number and the dots on the line represent the starting point of trajectory interruption or identity change. GT ID represents the actual ID. The number in the legend represents the trajectory number rather than GT ID. The legend also reflects the total number of trajectories in the sequence.

or without CMC, we find that CMC brings benefits for occlusion-aware framework in HOTA. When CMC is not used, the HOTA and MOTA performance is improved by 0.31% and 0.64% from Hybrid-SORT to OA-SORT. In contrast, HOTA and MOTA enhancement with CMC is 0.39%

CMC	Method	MOTA	HOTA	AssA	IDF1	IDS
✓	Hybrid-SORT	75.65	66.75	68.36	77.64	250
	Hybrid-SORT	76.21	67.83	70.15	80.25	204
✓	OA-SORT	76.29 (+0.64)	67.06 (+0.31)	68.74	78.19	239
	OA-SORT	76.75 (+0.54)	68.22 (+0.39)	70.73	80.93	170

Table 13. The influence of CMC on MOT17-val.

and 0.54%.

8.3. Additional data visualization under Occlusion

According to Fig. 1, the additional data, IDF1 and MOTA, are provided as shown in Fig. 7. Although the HOTA in the #0026 sequence has decreased, both IDF1 and MOTA have improved, especially in terms of MOTA, which has increased by approximately 1.4%. Combing Fig. 1, the results show that the main reason for this situation may be that the proposed occlusion-aware framework focuses on instantaneous states rather than long-term, resulting in unstable tracking.

8.4. MOT20 test set

In Tab. 14, the results under MOT20 [10] are presented. OA-SORT maintains good performance. Compared with Hybrid-SORT, OA-SORT improves with 0.4 IDF1 and 0.3 AssR. The results indicate that OAO and BAM can still maintain performance in dense-occlusion scenarios.

8.5. Visualization

We analyze a video segment from the DanceTrack0005 under Hybrid-SORT and OA-SORT, as shown in Fig. 8 and Fig. 9. In frame 66 (in Fig. 8), Hybrid-SORT fails to maintain IDs of #3 and #2 due to position cost confusion brought by occlusion. In contrast, OA-SORT can stable their IDs utilizing OAO. However, occlusion-aware framework is difficult to handle severe inaccurate detection under strong competition, as shown for bounding box #4 and #5 in the Fig. 10.

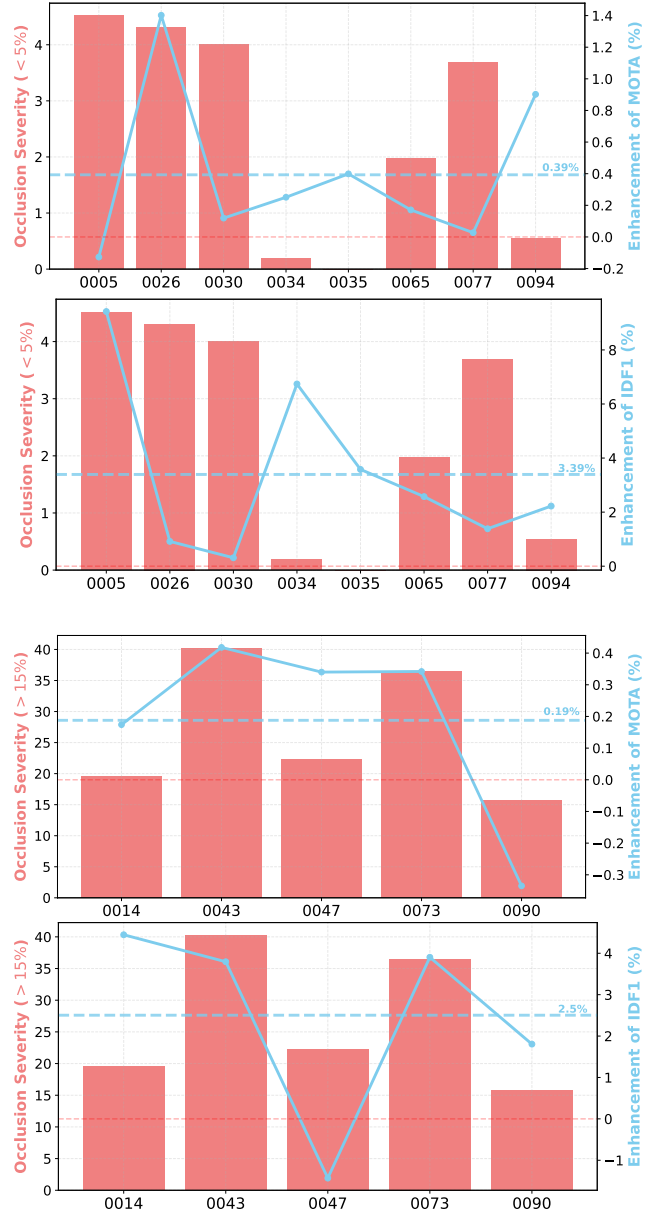
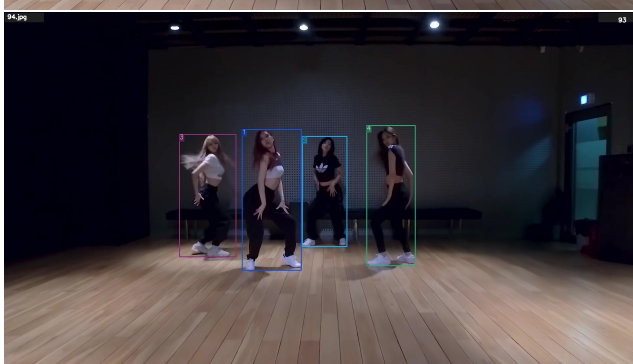
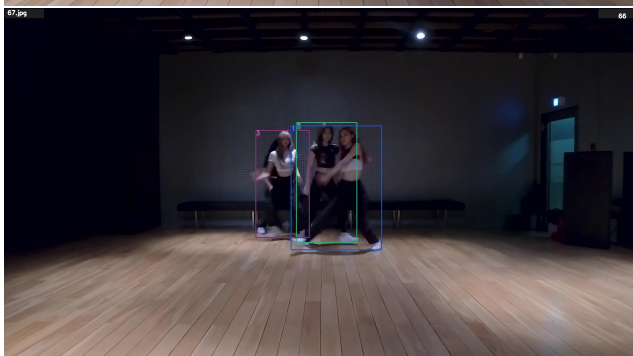
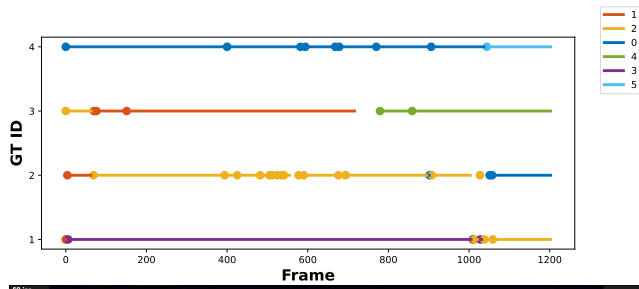


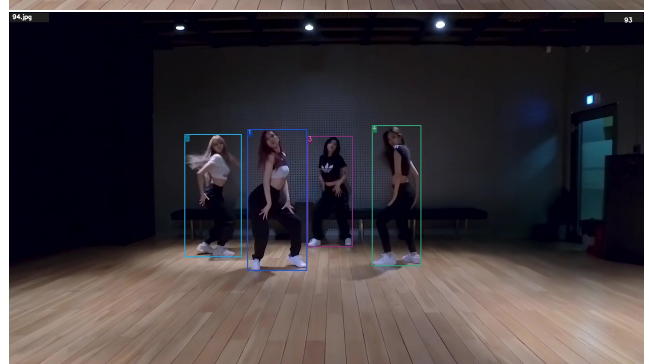
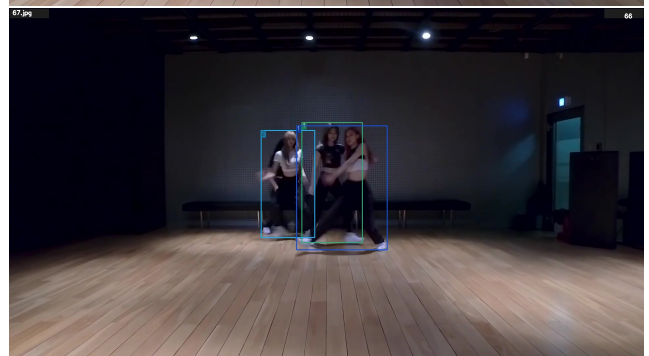
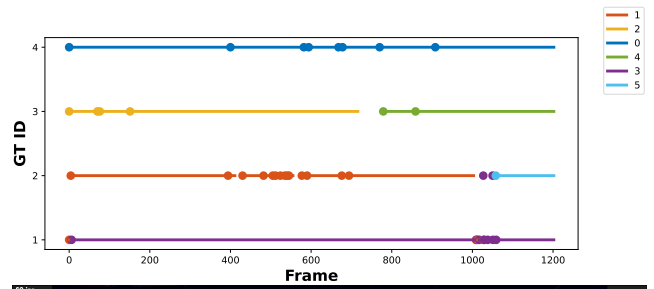
Figure 7. Performance improvement in MOTA and IDF1 over Baseline on the DanceTrack validation set under high and low occlusion severity.

Method	HOTA (%) \uparrow	MOTA (%) \uparrow	IDF1 (%) \uparrow	FP (10^4) \downarrow	FN (10^4) \downarrow	IDs \downarrow	AssA (%) \uparrow	AssR (%) \uparrow
FairMOT [61]	54.6	61.8	67.3	10.30	8.89	5,243	54.7	60.7
CSTrack [29]	54.0	66.6	68.6	2.54	14.4	3,196	54.0	57.6
TransMOT [8]	61.9	77.5	75.2	3.42	8.08	1,615	60.1	66.3
UTM [59]	62.5	74.3	79.8	3.00	8.15	1,228	-	-
GHOST [44]	61.2	73.7	75.2	-	-	1,264	-	-
ByteTrack [62]	61.3	77.8	75.2	2.62	8.76	1,223	59.6	66.2
OC-SORT [6]	62.1	75.5	75.9	1.80	10.8	913	62.0	67.5
StrongSORT [12]	61.5	72.2	75.9	-	-	1,066	63.2	-
AIPT [63]	62.1	76.9	75.4	2.10	9.80	1,134	61.1	-
Hybrid-SORT [58]	62.5	76.4	76.2	3.59	8.50	1,300	62.0	68.4
OA-SORT	62.6	76.5	76.6	3.59	8.46	1,274	62.1	68.7

Table 14. Results on MOT20-test with the private detections.

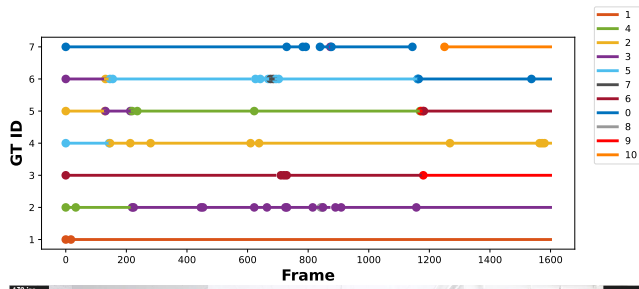


(a) The results through Hybrid-SORT.

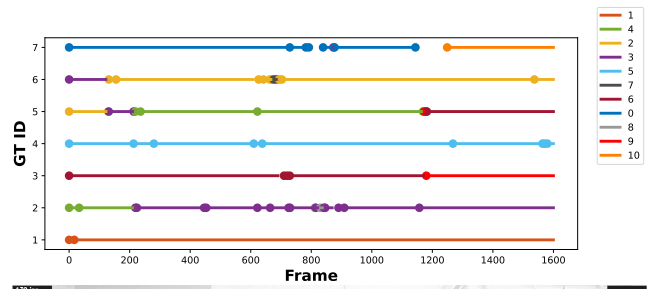


(b) The results through OA-SORT.

Figure 8. The results on DanceTrack0058. The different color indicates different trajectory number and the dots on the line represent the starting point of trajectory interruption or identity change. GT ID represents the actual ID. The number in the legend represents the trajectory number rather than GT ID. The legend also reflects the total number of trajectories in the sequence.



(a) The results through Hybrid-SORT.



(b) The results through OA-SORT.

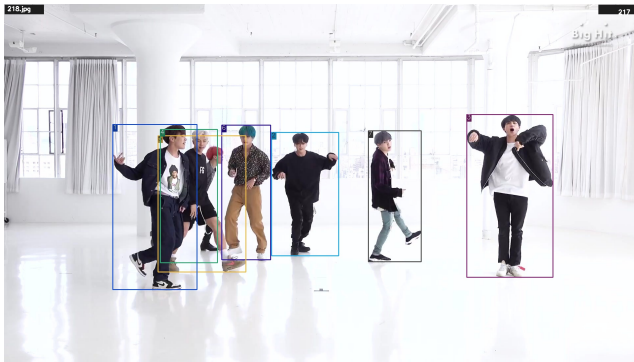
Figure 9. The results on DanceTrack0058. The different color indicates different trajectory number and the dots on the line represent the starting point of trajectory interruption or identity change. GT ID represents the actual ID. The number in the legend represents the trajectory number rather than GT ID. The legend also reflects the total number of trajectories in the sequence.



(a) Frame 215



(b) Frame 216



(c) Frame 217



(d) Frame 218

Figure 10. The failure case on DanceTrack0058. In Frame 217, due to the inaccurate detections of #4 and #5, the occlusion processing failed.